

# Observations on the controllability of motion of two-wheelers

K A Seffen<sup>1\*</sup>, G T Parks<sup>2</sup> and P J Clarkson<sup>2</sup>

<sup>1</sup>Applied Mechanics Division, Department of Mechanical Engineering, University of Manchester Institute of Science and Technology, Manchester, UK

<sup>2</sup>Engineering Design Centre, Department of Engineering, University of Cambridge, UK

**Abstract:** This paper presents an investigation into the motion of two-wheelers: everyday motorcycles and bicycles. The emphasis is on controllability of the system for small lateral deviations from straight running under idealized rider control. After introduction, a discussion of the kinematics, assumptions and geometry of a rider-vehicle system is presented, followed by a statement of the equations of motion. The control systems analogy is briefly reviewed, and state space methods formalize the concept of controllability. The difficulty in steered riding is quantified by the ratio of maximum to minimum singular values of the controllability Grammian and rideability is investigated for different designs of (a) a motorcycle from a well-known study and (b) a bicycle from a recent investigation. New insight into controlled two-wheeler behaviour is shown, compared with traditional methods, and can provide another means to design for a safety of vehicle performance.

**Keywords:** motorcycle, bicycle, lateral deviation, state space, controllability, rideability

## NOTATION

$a, c, d, e, f$	terms for location of the front-wheel hub and steering set mass centre relative to $O'$	$M_f, M_r, M_u, M_1, M$	mass of steering set, rear frame, upper torso, lower torso and complete system respectively
<b>A, B</b>	matrices for state space representation	<b>M, N, P, G</b>	matrices for second-order equations of motion
$C_{fc}, C_{rc}$	front- and rear-wheel cambering stiffnesses	$O, O'$	fixed inertial origin and moving reference origin in the ground plane respectively
$C_{fs}, C_{rs}$	front- and rear-wheel cornering stiffnesses	$OXYZ, Oxyz$	fixed orthogonal axes at $O$ and moving local body axes respectively
$D$	rideability index	$Q_i, q_i$	generalized force and generalized coordinate respectively
$g$	acceleration due to gravity	<b>Q</b>	controllability Grammian
$h, p$	lever arms of first moment of mass of the vehicle and the rider about horizontal and vertical directions at $O'$	$R_f, R_r$	front- and rear-wheel radii respectively
$(h_f, p_f)$	coordinates of $M_f$ relative to $O'$	$t_r$	front-wheel trail
$(h_1, p_1), (h_u, p_u)$	coordinates of $M_1$ and $M_u$ respectively relative to $O'$	$T, V$	total kinetic energy and potential energy respectively
$h_r$	height of $M_r$ above the ground	$v$	forward speed of vehicle and rider
$I, i$	moment or product of inertia and spin polar moment of inertia respectively	$w, L, b$	wheelbase parameters
		$\dot{x}, \dot{y}$	forward and lateral speed respectively of $O'$
		<b>X</b>	vector of state variables
		$Y_f, Y_r$	side forces at the front and rear wheels respectively
		$Z_f, Z_r$	vertical reactions at the front and rear wheels respectively

The MS was received on 8 May 2000 and was accepted after revision for publication on 27 September 2000.

\* Corresponding author: Applied Mechanics Division, Department of Mechanical Engineering, University of Manchester Institute of Science and Technology, Sackville Street, Manchester M60 1QD, UK.

$\gamma_s$	steer damping
$\delta, \phi, \psi$	steer, lean and yaw degrees of freedom respectively
$\epsilon$	rake angle of steering set

## 1 INTRODUCTION AND REVIEW

The ability of two-wheelers (bicycles and motorcycles) with seated riders to remain close to vertical during running has fascinated scientists and enthusiasts alike for many years, and authored articles span a century to date. The type of motion considered in this study is the lateral deviation of a rider and vehicle from the forward-moving and upright configuration. In particular, vehicle control is addressed; the rider applies a steering torque through the handlebars in response to perturbations in the motion, in order to restore the machine to vertical.

Relevant studies on two-wheeler control in the literature have been almost entirely devoted to motorcycle design and safety of handling. In contrast, important studies on bicycle stability have mainly considered ‘open-loop’ or free motion characteristics. Historically, the latter approach first provided valuable insight into self-stabilizing mechanisms without rider intervention [1, 2] and some early studies attempted to elucidate contributory factors to the build-up of potentially destabilizing frame oscillations at higher than normal speeds [3, 4]. Analysis usually involved the solution of a set of coupled differential equations of motion [5] for an often simplified idealization of a rider and bicycle; a key assumption was pure rolling of each wheel without slip.

With the advent of more powerful and faster motorcycles, better understanding of free motion was afforded through emergent techniques in linear systems theory, through realistic descriptions of tyre-ground interaction, and through a more accurate representation of machine make-up [6]. Key eigenmodes in lateral perturbation were identified as ‘capsize’, ‘weave’ and ‘wobble’, dominated by roll and yaw of the rear frame and by angle of steer relative to the rear frame respectively.

In practice, rider control is a continuous ‘closed-loop’ process, which couples the rider’s perception of vehicle response to a set of body torques applied by the rider to the machine at the handlebars, the saddle and the foot pedals through complex neuromuscular activity. The rider reacts, primarily, to visual cues in the immediate environment, in order either to compensate for errors between perceived motion and a desired response or to perform ‘a learned manoeuvre in an open-loop way’ [7].

In attempting to model this behaviour, analysis is uniquely complicated by the significance of the rider mass in the system, by its coupling to the vehicle and, hence, by its contribution to the total lateral inertia. A simple analogy is maintaining an inverted pendulum upright by controlling a sideways movement of its base [8]. The system has two degrees of freedom: the rotation

from vertical corresponds to a lean angle for the combined mass centre of rider and vehicle; the base velocity is expressed in terms of the forward speed and angle of steer of a hypothetical vehicle. A control law relates the lean angle to lateral movement by assuming that the rider steers in proportion to lean, and closed-loop control of the pendulum permits insight into the rider-vehicle interaction.

More accurate studies insert the equations of motion for a rider-vehicle system between points of ‘output’ and ‘input’. The input comprises the rider body torques; the output replicates the way in which a rider senses vehicular motion and is available for feedback to the input. The corresponding closed-loop architecture simulates a comparison of the amplified motion with reference levels by the rider to generate then the proper correcting action. The closed-loop equations of motion may be solved to give a time-varying prediction [9] or, more typically, efficient techniques available from linear systems are used to extract performance data. The latter approach requires specification of the problem either in the Laplacian domain or as a state space model. In two-wheeler analyses, the first of these methods has been employed to a great degree through Bode and Nyquist plots [7] and manipulation of transfer function poles [6, 9–12]; state space methods have been less used. However, irrespective of the choice of formulation, once an accurate model of the system dynamics has been established, vehicle and rider properties may be altered in any ensuing analysis. A designer may then perform virtual testing of different two-wheelers to address the variation in performance between vehicles, in order to enhance safety. Some important studies include a system of multiple loops and time delays to correspond to a number of rider response modalities with finite reaction times [7], control of non-linear equations of motion in which the rider has a finite frontal visibility [12] and adaptive rider control in pursuit of stabilized behaviour from some particular initial perturbation in the motion [9]. Improved modelling of vehicle realism has also been made possible through development of multi-body software packages [13].

Overall, the behaviour of two-wheelers has been well understood. However, one state space technique that is not employed during design is the concept of *controllability*. Although Section 4 discusses the concept in more detail, the controllability of any system describes the influence the input has upon altering the system ‘states’. The output is not considered and knowledge of a closed loop is, therefore, not needed. Moreover, when the input is described by a controlling element and the system states correspond to degrees of freedom of motion, controllability reflects the potential effectiveness of the controller in maintaining dynamic equilibrium or restoring it from some perturbed state. The technique has been successfully applied to vibration control in smart structures systems [14] and was extensively used by

Ackermann [15] to determine the conditions when control becomes ineffectual in automotive systems with uncertain parameters. One such example deals with automated four-wheel steering of a motorcar whose total mass depends on the number of passengers. The front and rear wheels are connected to a controlling torque actuator and loss of control is shown to take place at a velocity related to the inertia characteristics of the vehicle and its occupants. Hence, by redesigning the vehicle make-up to take account of this, the controller can be made to be effective over a greater range of speeds.

For a system describing the lateral perturbation dynamics of a two-wheeler with rider torques as input, controllability indicates the straight-line 'rideability' of the vehicle and the ability of the rider to alter the motion, in particular, to prevent an unstable open-loop behaviour. Note that, without reference to the rider interpretation of vehicle response, controllability does not formally assess the mental agility needed to perform continuous and sustained control over time. However, compared with traditional transfer function methods, this apparent drawback can be useful in a design context: first, the variation in cognitive ability *between* riders is not gauged and the controllability of a particular two-wheeler is the same for any rider, provided that the input is assumed to be the same; second, since the output does not feature, there are fewer 'design' variables and the problem of comparing the controllability of different vehicles is reduced. Therefore, it would seem advantageous to pursue a formulation of controllability for two-wheelers; this remains the focus of the rest of this study. The underlying ideas have been developed by Seffen [16].

First, the following section develops equations of motion for a simplified rider-two-wheeler model that captures key geometric features and a realistic tyre response. The equations of motion are then recast as a linear system of first-order equations using a state space representation. Controllability is formally introduced and a numerical index that quantifies the difficulty in riding is presented. The performance of various designs of motorcycle studied by Sharp [6] in an open-loop context are compared using this index. The variation in the rideability of a rider-bicycle system due to changes in parameters from an investigation into bicycle self-stability is also explored. This study concludes with a summary and avenues of further work.

## 2 EQUATIONS OF MOTION

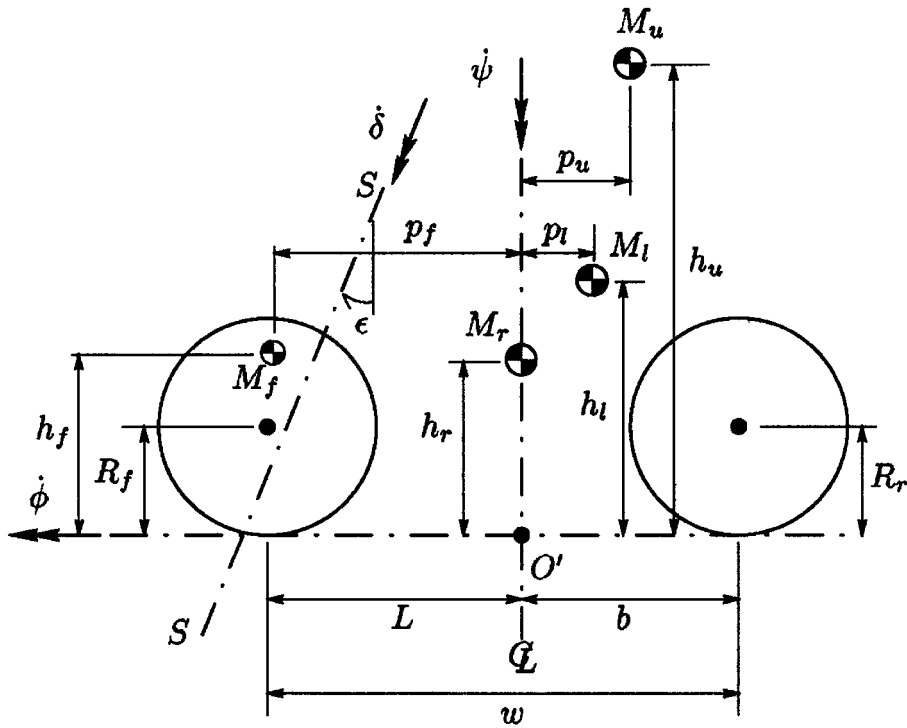
Traditional study considers either a bicycle or a motorcycle, with a rider, as a system of interconnected articulating rigid bodies and disks for wheels, in order to formulate the equations of motion. Despite obvious differences in size, power development and top speed

between bicycles and motorcycles, the basic layout, after Sharp [6], consists of a steering set that may be rotated relative to a rear frame by a rider sitting in front of a non-steerable rear wheel. The system is shown as vertical with the steering set in neutral in Fig. 1a. To account for a forward sweep and bend of most wheel forks, the angle of rake of the steer axis SS is  $\epsilon$  and the front-wheel hub offset to this axis is  $c$  [see Fig. 1b(i)]. Note that a positive trail  $t_r$  denotes the distance in a direction normal to SS and the projected axis of steer lies ahead of the wheel-ground contact point.

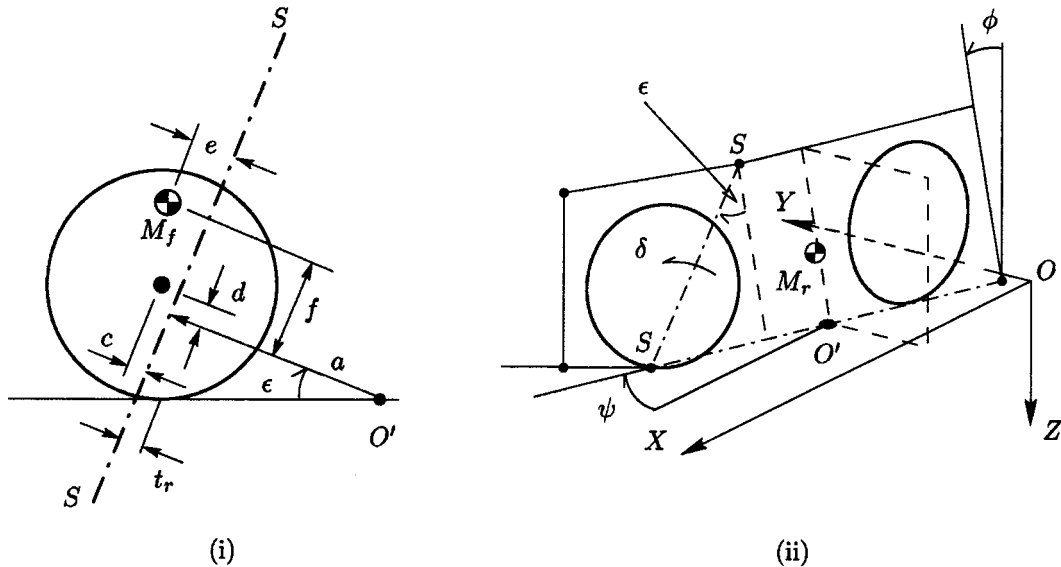
There are four rigid bodies of mass  $M_r$ ,  $M_f$ ,  $M_u$  and  $M_l$ , and the subscripts r, f, u and l denote the rear frame assembly including the rear wheel, the steering set with front wheel, the upper torso and lower torso of the rider respectively. The centroidal coordinates of each body relative to  $M_r$  in the same longitudinal plane are indicated in Fig. 1a. The distribution of mass in the upright system is assumed to be symmetric transverse to this plane but not within it. Hence, each body is modelled with a single in-plane product of inertia and three orthogonal moments of inertia referenced to a set of right-handed axes,  $Oxyz$ , fixed at its centroid. A compact notation uses  $I$  and a first subscript distinguishes between bodies, as for mass. Following this, moment of inertia directions are subscripted by  $xx$ ,  $yy$  and  $zz$  and correspond to axes  $Ox$ ,  $Oy$  and  $Oz$ ; for the product of inertia,  $xz$  relates to the  $Oxz$  plane. When the system is perfectly upright (Fig. 1a), for  $M_r$ ,  $M_u$  and  $M_l$ , the  $Oxy$  plane is horizontal with the  $Oz$  axis acting vertically downwards and  $Ox$  pointing along the frame from the rear to front; axes associated with  $M_f$  are rotated about  $Oy$  by the positive rake angle  $\epsilon$  so that  $Oz$  points along SS to ground. Point  $O'$  divides the wheelbase  $w$  into lengths  $L$  fore and  $b$  aft. The front and rear wheels, of radii  $R_f$  and  $R_r$  respectively, rotate relative to the front forks and to the rear frame and are each furnished with transverse spin polar moments of inertia,  $I_{fwy}$  and  $I_{rwy}$ .

A general perturbed configuration of the system from vertical and relative to a set of fixed inertial axes,  $OXYZ$ , is shown in Fig. 1b(ii). The rider is rigidly fixed to the rear frame, and out-of-plane upper-body lean, together with asymmetric posturing of the hips relative to the seat, is not considered. Thus,  $M_r$ ,  $M_u$  and  $M_l$  are always located in the same plane that undergoes small yaw and lean rotations,  $\psi$  and  $\phi$ , about axes  $OZ$  and  $OY$  respectively. The steering set rotates, in addition, by angle of steer  $\delta$  clockwise about SS. Point  $O'$  now tracks the intersection of the displaced plane of  $M_r$  with a transverse vertical plane through its centroid in the ground plane  $OXY$ , and its velocity is given by quasi-coordinates  $\dot{x}$  parallel to, and  $\dot{y}$  normal to, the rear frame. For a constant forward speed  $\dot{x} = v$ , the lateral degrees of freedom are fourfold;  $\dot{y}$ ,  $\dot{\psi}$ ,  $\dot{\delta}$  and  $\dot{\phi}$ . Some of the assumptions associated with the model are now discussed.

Pitching of the vehicle under lateral motion is neglected and is largely justified by only considering small



(a) Side view of upright two-wheeler and coordinates of each rigid body centre of mass relative to  $O'$ . Note axes of angular velocity of yaw,  $\psi$ , of roll,  $\phi$ , and of steer,  $\delta$



(b) (i) Geometry associated with steering set in upright, neutral position; (ii) displaced orientation of longitudinal plane of two-wheeler and associated angles of rotation. Transverse plane through  $M_r$  shown by thin, dashed lines

Fig. 1 Orientation of rider-vehicle system and associated geometry

displacements and rotations in each degree of freedom [6, 16]. Instantaneous tyre side-forces at the point of ground contact are determined from angles of side slip and camber for each wheel, which is assumed to roll without slip in the longitudinal direction of the rear

frame. Note that tyre relaxation effects are not implemented. The effects of aerodynamic drag and of relative motion between rider body parts are also not addressed. In the first case, the inclusion of air drag may not be a worthy consideration for bicycles

with open frames and spoked wheels moving at low speeds but cannot be ignored for faster motorcycles. Much work has been devoted to determining drag coefficients for racing cyclists and machines [17] and some data are available for motorcycles [18]. In the second case, a motorcycle rider executes small arm-to-hand motion during steering, whereas a cyclist moves virtually all body parts [19], even during relaxed pedalling. The rotary motion of the cyclist's legs further complicates analysis due to its dependence upon the pedal-crank angle, upon the gear ratio between the pedals and rear sprocket set and ultimately upon the rotation of the rear wheel. A compromise is to use an 'averaged' fixed layout for the legs and the arms with respect to the rear frame, as adopted by Wang and Hull [20, 21].

The governing equations of motion are derived by application of Lagrange's equations [22] and have been detailed at length by Seffen [16] following Sharp [6]; kinetic and potential energy expressions are stated in the Appendix. Differentiation was automatically performed by employing the symbolic computation capabilities of MATLAB [23] to reduce the chance of human error and to compute linearized equations.

The resulting set of four second-order differential equations of motion is compactly written as

$$\mathbf{M} \begin{bmatrix} \ddot{y} \\ \ddot{\psi} \\ \ddot{\delta} \\ \ddot{\phi} \end{bmatrix} + \mathbf{N} \begin{bmatrix} \dot{y} \\ \dot{\psi} \\ \dot{\delta} \\ \dot{\phi} \end{bmatrix} + \mathbf{P} \begin{bmatrix} \delta \\ \phi \end{bmatrix} + \mathbf{G}[\tau_s] = \mathbf{0} \quad (1)$$

where  $\tau_s$  is a steer input torque applied by the rider to the handlebars along SS; to simplify matters, other body torques such as an upper body lean [7] and a longitudinal pedal torque [9] are not included. The linear time-invariant matrices of mass, damping, stiffness and input,  $\mathbf{M}$ ,  $\mathbf{N}$ ,  $\mathbf{P}$  and  $\mathbf{G}$  respectively, are defined by

$$\mathbf{M} = \begin{bmatrix} M & Mp & M_f e & Mh \\ Mp & I_{O'zz} & I_1 & -I_{O'xz} \\ M_f e & I_1 & I_{fss} & I_2 \\ Mh & -I_{O'xz} & I_2 & I_{O'xx} \end{bmatrix} \quad (2)$$

$$\mathbf{N} = v \begin{bmatrix} \frac{C_1}{v^2} & \frac{-wC_2}{v^2} + M & \frac{-t_r C_{fs}}{v^2} & 0 \\ \frac{-wC_2}{v^2} & \frac{w^2 C_5}{v^2} + Mp & \frac{-t_r LC_{fs}}{v^2} - \frac{i_{fwy} \sin \epsilon}{R_f} & \frac{-I_{fss}}{r} \\ \frac{-t_r C_{fs}}{v^2} & -\frac{t_r LC_{fs}}{v^2} + M_f e + \frac{i_{fwy} \sin \epsilon}{R_f} & \frac{t_r^2 C_{fs}}{v^2} + \frac{\gamma_s}{v} & \frac{-i_{fwy} \cos \epsilon}{R_f} \\ 0 & Mh + \frac{I_{fss}}{r} & \frac{i_{fwy} \cos \epsilon}{R_f} & 0 \end{bmatrix} \quad (3)$$

$$\mathbf{P} = \begin{bmatrix} -C_3 & -C_4 \\ -LC_3 & -wC_6 \\ t_r C_3 - M_j g e \sin \epsilon & t_r C_{fc} - M_j g e \\ -M_j g e & -Mgh \end{bmatrix} \quad (4)$$

$$\mathbf{G} = [0 \quad 0 \quad -1 \quad 0]^T \quad (5)$$

where the superscript T denotes vector transpose. A full description of all terms is given in the Appendix.

### 3 STATE SPACE MODEL AND CONTROLLABILITY

The equations of motion are now recast as a set of coupled first-order equations using the method of *state space* from linear systems theory [24]. The elements of a state variable vector  $\mathbf{X}$  are motion coordinates and velocities, such that

$$\mathbf{X} = [\delta \quad \phi \quad \dot{y} \quad \dot{\psi} \quad \dot{\delta} \quad \dot{\phi}]^T \quad (6)$$

and the set of equations described in equation (1) may now be rewritten

$$\dot{\mathbf{X}} = \mathbf{A}\mathbf{X} + \mathbf{B}\mathbf{U} \quad (7)$$

with input vector  $\mathbf{U} = [\tau_s]$ . The linear time-invariant matrices  $\mathbf{A}$  and  $\mathbf{B}$  are given by

$$\mathbf{A} = \begin{bmatrix} \mathbf{0}_{2,4} & \mathbf{I}_{2,2} \\ -\mathbf{M}^{-1}\mathbf{P} & -\mathbf{M}^{-1}\mathbf{N} \end{bmatrix}, \quad \mathbf{B} = \begin{bmatrix} \mathbf{0}_{2,1} \\ -\mathbf{M}^{-1}\mathbf{G} \end{bmatrix} \quad (8)$$

following Newland [25]; submatrix dimensions for zero and identity matrices,  $\mathbf{0}$  and  $\mathbf{I}$  respectively, are indicated in the subscripts. The concept of controllability is now introduced, followed by a strict algebraic formulation.

From Friedland [24], a system is said to be controllable if all its state variables can be affected, to some degree, by the input. Conversely, if some or all of its states are detached from the input, these states form an uncontrollable subsystem. However, if the open-loop response of the system is asymptotically stable, any uncontrollable states decay harmlessly to zero and are said to be *stabilizable*. More importantly, an unstable system with uncontrollable subsystems cannot be stabilized. Physically uncontrollable systems arise in the

following situations. If the system is defined by extra degrees of freedom that are not connected to the input and that, however, behave in an unstable fashion, then the amplitudes of these redundant states grow in a divergent manner irrespective of the input performance. Uncontrollability also occurs when the controlling forces and torques are internal; most simply, the linear (and angular) momentum of the system cannot be altered by the input. Another occurrence takes place in systems with symmetry, such as ‘balanced’ electrical bridge networks. The interchange of energy between states may become disconnected from the input when parameters within the system adopt certain values, and those states are not influenced by the input.

Formalizing controllability requires, first, the following Gramian (matrix) definition [24]. Using the matrices in equation (7) define

$$\mathbf{Q} = [\mathbf{B} \quad \mathbf{AB} \quad \cdots \quad \mathbf{A}^{k-1}\mathbf{B}] \quad (9)$$

where  $k$  is the order of the system and equal to the number of state variables. For the system described by equation (7) to be controllable, the rank of matrix  $\mathbf{Q}$  must be equal to  $k$ ; if the rank is less than  $k$ , the system is uncontrollable. A further embellishment is that singular values are indicative of matrix rank. Therefore, the system is also uncontrollable if the lowest singular value is zero. If this is not the case, the ‘degree’ of controllability may be given by the ratio of highest singular value  $S_{\max}$  to lowest singular value  $S_{\min}$  of  $\mathbf{Q}$ , as first noted by Friedland [26] and later developed by Moore [27]. In essence, as this ratio becomes larger, it is more ‘difficult’ to influence the system states; for two-wheelers, this would correspond to decreasing rideability for the vehicle. Therefore, an ‘index’  $D$  associated with the difficulty in riding may be defined by

$$D = \log_{10} \sqrt{\frac{S_{\max}}{S_{\min}}} \quad (10)$$

The square root was suggested by Furuta *et al.* [28], and  $\log_{10}$  is used for sensible scaling.

A final point concerns the performance of the singular values of  $\mathbf{Q}$  according to the amplitude of input torque  $\tau_s$  in equation (5). If, instead, this amplitude is not equal to unity, it can be shown that all singular values linearly scale with the amplitude. The ratio in equation (10) still remains the same provided that the lowest singular value is not zero and, hence, for a controllable system, the magnitude of  $D$  is independent of the size of torque. Physically, the ‘muscular’ strength of the rider is not taken into account in the above formulation; for different amplitudes of torque, the time taken to alter the states does, however, change. A corollary to this is an intermediate step in the derivation of controllability from Friedland [24], which assumes that the time taken

to affect the states is solely not an infinite quantity for a system to be controllable.

#### 4 INVESTIGATION OF THE RIDEABILITY OF TWO-WHEELERS

The following sections now present the rideability of some two-wheelers. This is achieved by, first, evaluating  $\mathbf{M}$ ,  $\mathbf{N}$  and  $\mathbf{P}$  in equations (2) to (4) over a range of speeds for a specific design, and then by substituting these matrices into equation (8) to determine  $\mathbf{A}$  and  $\mathbf{B}$ . Inserting these matrices into  $\mathbf{Q}$  via equation (9),  $D$  is then computed using equation (10) and the process is repeated for each new vehicle. Note that singular values were obtained by digital computation using the software package MATLAB [23].

To explain the controllability profile for each design the following approach is proposed. Recall that, informally, a controllable system has all its states affected by the input. The natural tendency of the system is to behave according to its eigenmode response. The performance of the input torque is, therefore, in direct competition with the dominant modes and their associated damping and oscillation frequencies. Hence, for a given vehicle, this would suggest that, in general, as the free motion response becomes increasingly less stable, controllability becomes more difficult, and a comparison of  $D$  with eigenmodal behaviour is appropriate. For a change in vehicle design, it is also appropriate to consider how this alteration affects the torque in terms of the change to other physical factors that may compromise or enhance the effect of the torque. These arguments are now applied to, first, a motorcycle.

##### 4.1 Motorcycles

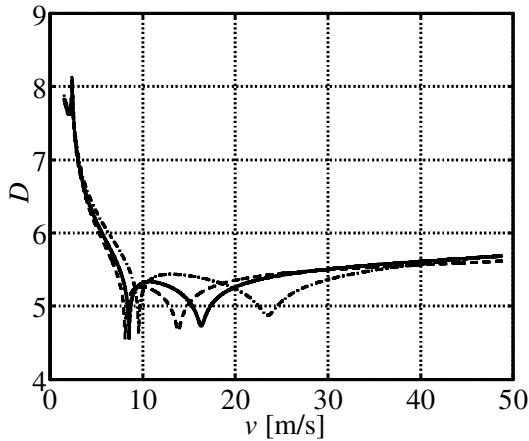
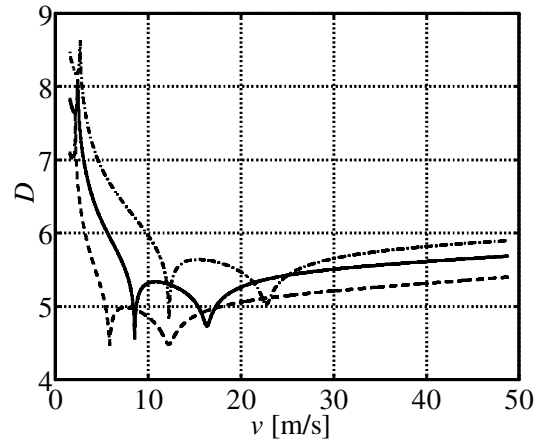
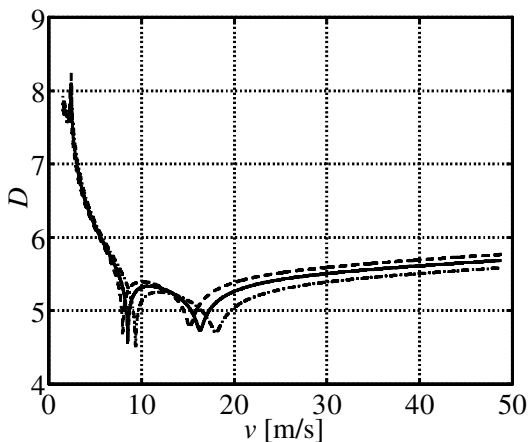
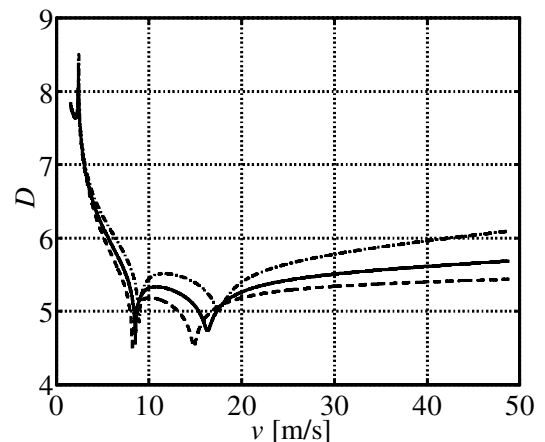
The standard machine and the range of speeds are the same as those used by Sharp [6]; Table 1 lists vehicle and rider metric properties. Note that it is presumed that the rider properties from Sharp are grouped together with those of the rear frame and, thus, terms associated with the bodies of masses  $M_1$  and  $M_u$  do not appear.

Figure 2 indicates a continuous variation in  $D$  as a function of speed  $v$ ; each part of the figure deals with three types of machine: the standard motorcycle, and two layouts that have been altered according to changes in the steering set proposed by Sharp [6].

For the standard machine curve, it can be clearly seen that, in general, as the speed increases from zero, the motorcycle becomes easier to control until  $v \approx 25$  m/s where the difficulty in riding begins to increase. Somewhere below mid-range speeds,  $D$  exhibits two sharp but continuous local minima and a single local maximum; this is also the trend for all other designs. Everywhere,  $D$  lies in the range between 4 and 9, and

**Table 1** Standard machine. Parameters with zero values are not stated. (From Sharp [6])

Parameter (units)	Value	Parameter (units)	Value	Parameter (units)	Value
$M_r$ (kg)	217.45	$M_f$ (kg)	30.65	$I_{rxx}$ (kg m <sup>2</sup> )	31.184
$I_{fxx}$ (kg m <sup>2</sup> )	1.234	$I_{fzz}$ (kg m <sup>2</sup> )	21.070	$I_{fzz}$ (kg m <sup>2</sup> )	0.442
$I_{fzz}$ (kg m <sup>2</sup> )	1.735	$i_{fwy}$ (kg m <sup>2</sup> )	0.719	$\lambda_{fwy}$ (kg m <sup>2</sup> )	1.051
$h_r$ (m)	0.615	$h_f$ (m)	0.467	$p_r$ (m)	0.854
$b$ (m)	0.480	$L$ (m)	0.935	$e$ (m)	0.0244
$c$ (m)	0.0226	$\epsilon$ (rad)	0.4712	$t_r$ (m)	0.1158
$R_r$ (m)	0.3048	$R_f$ (m)	0.3048	$\gamma_s$ (N m/rad s)	6.780
$C_{fs}$ (kN/rad)	11.1739	$C_{fc}$ (kN/rad)	0.9386	$C_{rs}$ (kN/rad)	15.8312
$C_{rc}$ (kN/rad)	1.3256				

(a) Steering damper  $\gamma_s$  with units of N m/rad/s: solid,  $\gamma_s = 6.780$ ; dashed,  $\gamma_s = 2.712$ ; dash-dot,  $\gamma_s = 13.558$ .(b) Trail: solid,  $t_r = 0.116$  m; dashed,  $t_r = 0.058$  m; dash-dot,  $t_r = 0.177$  m.(c) Rake angle: solid,  $\epsilon = 27^\circ$ ; dashed,  $\epsilon = 19^\circ$ ; dash-dot,  $\epsilon = 35^\circ$ .(d) Front wheel polar moment of inertia  $i_{fwy}$  with units of kg m<sup>2</sup>: solid,  $i_{fwy} = 0.719$ ; dashed,  $i_{fwy} = 0.359$  ( $\gamma_s = 4.067$ ); dash-dot,  $i_{fwy} = 1.437$  ( $\gamma_s = 10.169$ ).**Fig. 2** Effect on the index  $D$  for difficulty in riding by variation in (a) steer damping, (b) trail length, (c) rake angle and (d) front-wheel polar moment of inertia using parameters for motorcycles from Sharp [6]. All solid curves refer to controllability of a standard machine

nowhere is uncontrollability observed, i.e. the lowest singular value in equation (10) is never computed as zero. As a comparison, for upright control of a double inverted pendulum [28],  $D \approx 5.8$ . The free-motion behaviour of the motorcycle with instant tyre response from Sharp [6] exhibits a weave instability with increas-

ing damping in the range  $0 \text{ m/s} < v < 6 \text{ m/s}$ , followed by a divergent capsizing of a small but approximately constant damping above  $v = 10 \text{ m/s}$ ; as  $v$  increases towards maximum speed, there exists a well-damped but stable wobble that increases in frequency.

At low but increasing speeds, the rider torque becomes

more effective as the natural damping of the unstable weave mode increases and  $D$  rapidly descends as  $v$  tends towards 9 m/s; above this speed, the vehicle approaches unstable capsizes. The sharp upturn in  $D$  reflects a change in the sign of damping of the capsize mode, but  $D$  levels off quickly as this damping becomes constant, and  $D$  then decreases as the stable weave mode now becomes more heavily damped. At approximately  $v = 16.5$  m/s, the difficulty in riding rises again; from this stage until the maximum speed the weave and steer modes, although both stable, increase in frequency and decrease in damping, and  $D$  must increase.

Figure 2a deals with changes to the steering damping coefficient  $\gamma_s$ . The most notable effect upon rideability occurs when  $\gamma_s$  is increased; the second local minimum displaces to  $v \approx 24$  m/s and  $D$  is reduced for all speeds above  $v = 20$  m/s compared with the standard vehicle. Sharp [6] noted that during free motion of the vehicle with full tyre treatment, i.e. relaxation effects are taken into account, by increasing  $\gamma_s$ , adequate stability for wobble across all speeds is achieved at the expense of destabilizing the weave mode; the capsize mode remains relatively unaffected. A separate investigation by the present authors has shown that this is also true for instant tyre response. Therefore, more damping limits the build-up of steering oscillations at speeds above mid-range speeds, and the vehicle is easier to control, but it redirects excess energy into rigid body weave oscillation, which, at a relatively low speed, is the dominant mode and causes  $D$  to increase.

The variation in  $D$  with front-wheel trail is indicated in Fig. 2b; the rake angle is that of the standard machine,  $\epsilon = 27^\circ$ . Decreasing  $t_r$ , on average, makes control more effective and vice versa. Compared with the standard motorcycle, Sharp [6] recorded that too little trail slightly augments capsizes, while more trail has little effect upon the natural behaviour. These comments would suggest that  $D$  should be marginally greater for smaller  $t_r$ , especially during mid-range speeds where capsizes is the dominant mode, and that  $D$  is not much altered for a larger trail. However, the reason for the very noticeable departures in controllability is due to the change in moment of the tyre side force about the steer axis; when  $t_r$  is reduced, this moment, which opposes the input torque, is decreased, and the torque effect is augmented, resulting in better rideability throughout. For larger trail, the opposite effect take place.

Figure 2c is concerned with the angle of rake. The difference in controllability, compared with the standard machine, is approximately constant above  $v = 25$  m/s for both  $\epsilon = 19^\circ$  and  $\epsilon = 35^\circ$ , with the larger rake angle affording more effective control at higher speeds. There is not much difference in  $D$  across designs at low to mid-range speeds. When the rake angle is reduced, damping of the weave mode towards the top speed is reduced and control is more difficult; increasing  $\epsilon$  affords better weave damping beyond  $v = 18$  m/s and  $D$  is reduced.

Finally, Fig. 2d considers changes in  $i_{fwy}$ , the front-wheel polar moment of inertia. Note also the coefficients of steer damping used by Sharp [6]; these ensure that the wobble eigenmode is approximately the same as that of the standard machine.

For smallest  $i_{fwy}$ , the capsize mode is less severe, as recorded by Sharp [6], and controllability is improved during mid-range speeds. In contrast, the weave damping towards the top speed decreases compared with the case for largest  $i_{fwy}$  and yet the system is easier to control. This is due to gyroscopic effects; for a larger spin inertia, the gyroscopic torque, which opposes steer torque, is increased and controllability is reduced.

It can be clearly seen in the above study that, by making alterations to the steering set, the rideability is noticeably altered. In particular, by increasing the steer damping and by decreasing  $i_{fwy}$ , rideability is enhanced above mid-range speeds, whereas decreasing the trail results in better rideability across all speeds. Sharp [6] also considered other designs with increased wheelbase, a reduction in tyre contact stiffnesses and a modification to the centre-of-mass position of the steering set. The rideability of these machines is left as an exercise in further work; a second investigation is now carried out for a bicycle.

## 4.2 Bicycles

It is expected that the rideability of a bicycle, compared with a motorcycle, is different because it is less massive, has a lower top speed and possesses different tyre properties due to smaller-width wheels and is, therefore, now pursued. Bicycle rideability is also worthy of study since most persons have had experience of riding bicycles at some stage in their lives when they may not have ridden a motorcycle.

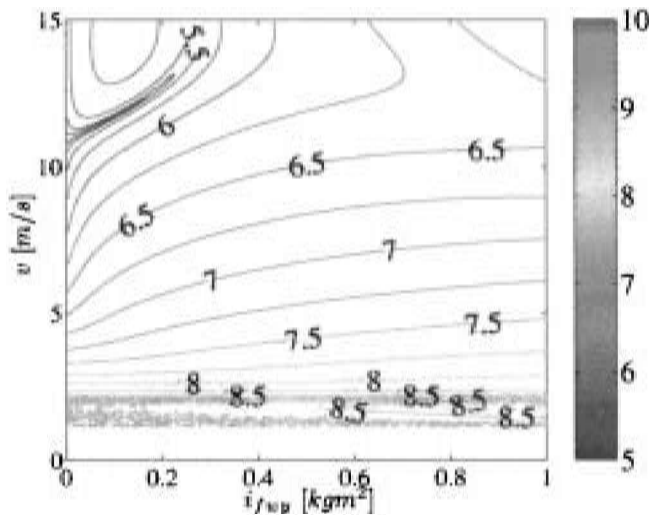
Rather than compare controllability with free-motion behaviour, this section quantifies experimental observations made by Jones [2] who attempted to construct an unrideable bicycle from key modifications to its steering set. For completeness, rideability profiles are presented as contours of  $D$  that vary continuously according to speed and to alteration; the top speed is chosen to be 15 m/s (33 mile/h).

Seffen [16] considered the main body of the rear frame as a planar classical diamond shape consisting of connected tube members; their dimensions are derived by a separate analysis for optimal frame layout in response to different pedalling loads [29]. The rider mass and geometry are modelled by a segmental mass approach for each body part following Wang and Hull [20, 21] and the standard bicycle properties are given in Table 2.

Figure 3 considers a variation in spin inertia of the steering set; typically,  $i_{fwy}$  is no greater than 0.5 kg m<sup>2</sup> for the average bicycle. The mass and radius of the front wheel are everywhere constant, together with moments

**Table 2** Parameter values for bicycle system. (From Seffen [16])

Parameter (units)	Value	Parameter (units)	Value	Parameter (units)	Value
$M_r$ (kg)	3.6016	$M_l$ (kg)	25.28	$M_u$ (kg)	54.59
$M_f$ (kg)	2.1551	$I_{r,xx}$ (kg m <sup>2</sup> )	0.2214	$I_{l,xx}$ (kg m <sup>2</sup> )	1.002
$I_{u,xx}$ (kg m <sup>2</sup> )	1.007	$I_{f,xx}$ (kg m <sup>2</sup> )	0.1034	$I_{r,zz}$ (kg m <sup>2</sup> )	0.3419
$I_{l,zz}$ (kg m <sup>2</sup> )	0.2330	$I_{u,zz}$ (kg m <sup>2</sup> )	1.5325	$I_{f,zz}$ (kg m <sup>2</sup> )	0.0458
$I_{r,zz}$ (kg m <sup>2</sup> )	-0.1757	$I_{l,zz}$ (kg m <sup>2</sup> )	0.1862	$I_{u,zz}$ (kg m <sup>2</sup> )	-0.8645
$I_{f,zz}$ (kg m <sup>2</sup> )	0.0051	$i_{f,wy}$ (kg m <sup>2</sup> )	0.09	$\lambda i_{r,wy}$ (kg m <sup>2</sup> )	0.09
$h_r$ (m)	0.5519	$h_l$ (m)	0.6921	$h_u$ (m)	1.1878
$h_f$ (m)	0.4251	$p_l$ (m)	-0.0661	$p_u$ (m)	-0.3797
$p_f$ (m)	0.5728	$b$ (m)	0.3367	$L$ (m)	0.6272
$e$ (m)	0.0175	$\epsilon$ (deg)	15	$c$ (m)	0.0376
$t_r$ (m)	0.04	$R_f$ (m)	0.3	$R_r$ (m)	0.3
$C_{fs,rs}$ (N/rad)	10.45  $Z_{f,r}$	$C_{fc,rc}$ (N/rad)	0.1095  $Z_{f,r}$		

**Fig. 3** Index  $D$  for a bicycle with variation in the polar moment of inertia of the front wheel and speed  $v$ 

of inertia in the wheel plane. Note that a constant-mass wheel with variable spin inertia is physically analogous to having a third wheel mounted close to the front wheel and clear of the ground that is free to rotate, as performed by Jones [2]. By altering its spin speed and direction, the net angular momentum of the steering set also changes and Jones was able to study the effects of the resultant change in gyroscopic precession applied to the steering set upon the ease of riding.

Note first in Fig. 3 that the smooth contour variation breaks down at speeds below approximately 2.1 m/s when  $D$  is greater than 8.5. The lowest singular value in equation (10),  $S_{\min}$ , erratically alternates between zero and a small positive number for minute changes in  $v$  and  $i_{f,wy}$ . Infinite values of  $D$  are ignored in the plotting procedure, in order to avoid scaling problems, and thus a 'band' of broken contours for  $D \approx 8.5$  is observed for  $1.2 \text{ m/s} < v < 2.1 \text{ m/s}$ . Below  $v = 1.2 \text{ m/s}$ ,  $S_{\min}$  is always computed as zero and infinite value contours are not drawn.

In the broken areas, although large values of  $D$  for nearby controllable configurations suggest a 'closeness' to uncontrollability, the behaviour is not confined to a

continuous variation in  $v$  and  $i_{f,wy}$ , as observed by Lopez-Linares *et al.* [14], and suggests a numerical instability during computation of singular values rather than an uncontrollable system. This is also confirmed in Figs 5 and 6 that are introduced later. In these figures, continuous contours of  $D \approx 10$  can just be seen below the broken contours; if the system were physically uncontrollable for all designs above the cut-off  $D \approx 8.5$ , then the re-emergence of continuous contours with even higher values of  $D$  would not be expected. The present authors were unsuccessful in resolving the problem; however, in all figures, perceived uncontrollability occupies a small portion of the results and is removed from the majority of consideration.

During controllable behaviour, Fig. 3 shows that a bicycle tends to become easier to control with increased speed. In the region  $2.1 \text{ m/s} < v < 10 \text{ m/s}$ , as  $i_{f,wy}$  increases, the rideability becomes less sensitive to gyroscopic effects. Above  $v = 10 \text{ m/s}$ , for lowest  $i_{f,wy}$ , the contours turn sharply towards the top of the figure, and  $D$  is almost independent of speed. When  $i_{f,wy}$  is largest, controllability depends on both  $v$  and  $i_{f,wy}$ . Therefore, for relatively low speeds, gyroscopic effects have minimal influence on controllability. Jones [2] also observed that his modified bicycle can be ridden quite easily, irrespective of the magnitude of and direction of spin of the extra wheel, even when the extra wheel is counter-spun to negate the possibility of gyroscopic precession.

Further experiments by Jones [2] indicate that the motion of a *riderless* bicycle is, however, very dependent on the angular velocity of the extra wheel and, hence, upon gyroscopic effects. This is replicated in Fig. 4 where the rider mass has been conveniently set to zero, although a steer input torque still prevails. Controllability is heavily influenced by both  $v$  and  $i_{f,wy}$  for the majority of the contours; only for  $v < 2 \text{ m/s}$  is the behaviour independent of spin inertia.

Figure 5 considers a variation in trail. The rear frame lay-out remains the same, but the geometry and inertia properties of the steering set are recalculated according to the change in position of the front wheel relative to the hub position of the standard bicycle. Ignoring the region of broken contours, rideability improves as  $v$

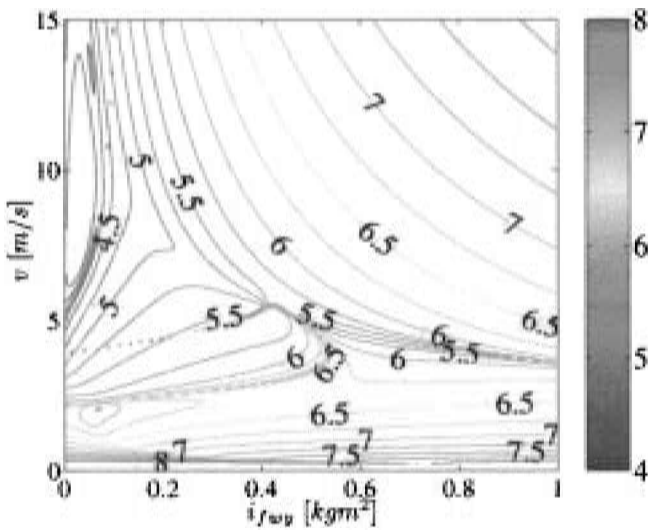


Fig. 4 Parameters as in Fig. 3, but the rider has zero mass

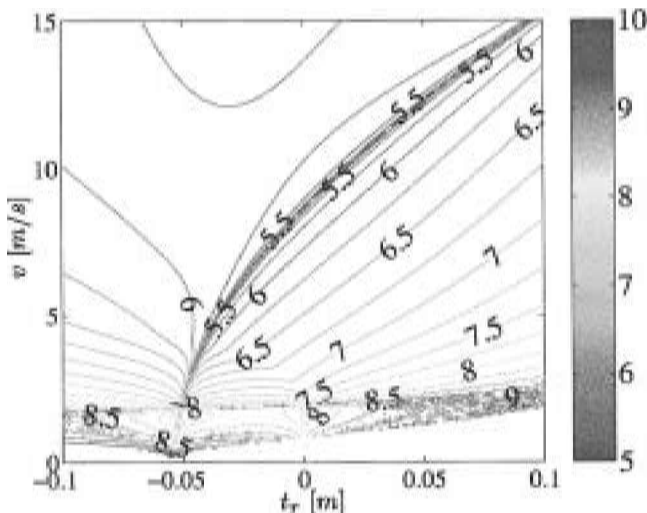


Fig. 5 Index  $D$  with variation in the trail for a bicycle and speed  $v$

increases for any design. At a given speed, as  $t_r$  becomes more positive, bicycle control becomes more effective until a minimum value of  $D$  is observed; thereafter, the difficulty in riding increases. This is also recorded by Jones [2] using two modified bicycles with augmented negative and positive trails: the first bicycle, as expected, was extremely difficult to ride; the second bicycle, according to Jones was 'awkward to ride, but incredibly stable if rider-less'.

In attempting to explain this behaviour, Jones identified the importance of a gravitational couple applied to the steering set under lean. If the trail is positive, then this couple causes the wheel to steer into the direction of lean and the couple is said to be self-stabilizing. Sometime later, Lowell and McKell [5] quantified the magnitude of 'Jones's couple' and it is a specialized form of the term  $M_{jge}$  given in the Appendix. Hence, moving from a negative to a positive trail, Jones's couple first

opposes the steer torque, but decreasingly so, and then acts in the same direction as the torque, increasing its effect, and  $D$  reduces. However, when  $t_r$  becomes larger, the lever arm of the tyre-side force now increases, causing a greater resistive moment to be applied about the steer axis, and controllability becomes more difficult. Note that there is no design that gives optimal behaviour, i.e. smallest  $D$  for the range of speeds. Modern-day bicycles employ a positive trail of a few centimetres.

A final aspect of study considers a finite response time from the rider; the input torque is pre-multiplied by a first-order Padé approximation [30] of time delay in state space form and  $D$  is then evaluated as before. The time lag in this analysis was set to 0.1 s following Weir and Zellner [7]. The results are displayed in Fig. 6 for the same range of trails as before; the contour profile is similar to that in Fig. 5, but with elevated values of  $D$  at a particular  $(t_r, v)$  position. Hence, the bicycle is more difficult to control.

## 5 SUMMARY AND CONCLUSIONS

The aim of this study has been to introduce the controllability concept associated with state space methods from linear systems, in order to investigate the rideability of two-wheelers. In particular, controllability has been formally quantified by means of matrix definition and by an associated index that describes the level of difficulty in perceived control of a generic system. This, in turn, has been applied to a compact set of equations that describe the lateral perturbation dynamics from the vertical upright running of either a motorcycle or a bicycle, with a seated fixed rider; the rider may only apply a steering torque for control. Several designs of motorcycle from Sharp [6] have been assessed for controllability. It has been shown that rideability is improved when the

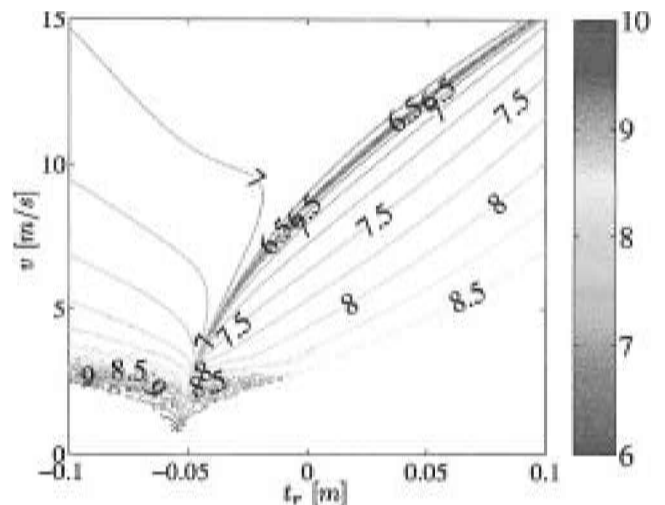


Fig. 6 Index  $D$  with variation in the trail and speed  $v$ ; the rider reaction time is 0.1 s

dominant free-motion eigenmodes become more damped or less oscillatory or when the changes made to the vehicle reduce those effects that oppose the input torque. The rideability of a bicycle has been explored by a systematic variation in the spin polar moment of inertia of the front wheel and the trail of the steering set; gyroscopic effects, although important at large speeds, do not greatly affect controllability at everyday riding pace, whereas rideability is more sensitive to trail. The importance of rider reaction time has been highlighted.

There are several points of discussion for closing. Usually, the application of controllability to a problem is accompanied by the concept of *observability*, which relates the ability of the controlling element to measure values of the output states. An unobservable system contains states that cannot be measured by the controller. Observability requires the formulation of an output that, in this study, corresponds to the rider interpretation of vehicle response. Even though there exists evidence to suggest that most riders react in a similar way during control [8], the study of observability is left as an exercise for further work when more data become available for a range of rider responses. It has also been noted that the computation of singular values is subject to the limit of numerical accuracy of the particular software package, which may lead to an incorrect interpretation of system controllability. More robust algorithms are being sought by the present authors to improve confidence in predicting controllability. Finally, there does not exist any simple way to ascertain conditions for optimal rideability experimentally other than when the vehicle 'feels' easy to ride and to manoeuvre. The issue is somewhat complicated by the absence of a time-dependent feature for controllability upon the alteration of states and, hence, simply to measure the variation in states with respect to time and input torque during riding does not suffice; the present authors would welcome any comments on this point.

## ACKNOWLEDGEMENTS

The authors gratefully acknowledge financial support from the Engineering and Physical Sciences Research Council (UK) (Grant GR/M23236) for this study. In addition, a debt of gratitude is offered to Professor R. E. Klein formerly of the University of Illinois, Urbana-Champaign, USA, and also to Professor R. S. Sharp, Cranfield University, UK, for many enlightening and explanative E-mails about aspects of their research into two-wheeler motion and control. Finally, the authors' colleague, Dr G. Papageorgiou of the Control Group, Department of Engineering, University of Cambridge, is thanked for his 'piecewise' introduction on linear systems theory to the primary author.

## REFERENCES

- 1 Timoshenko, S. and Young, D. H. *Advanced Dynamics*, 1948, pp. 239–243 (McGraw-Hill, New York).
- 2 Jones, D. E. H. The stability of the bicycle. *Physics Today*, April 1970, **23**(4), 34–40.
- 3 Whipple, F. J. W. The stability of the motion of the bicycle. *Q. J. Pure Appl. Math.*, 1899, **30**, 312.
- 4 Pearsall, R. H. The stability of the bicycle. *Proc. Inst. Automobile Engng*, 1922, **17**(395).
- 5 Lowell, J. and McKell, H. D. The stability of bicycles. *Am. J. Physics*, 1982, **50**, 1106–1112.
- 6 Sharp, R. S. The stability and control of motorcycles. *J. Mech. Engng Sci.*, 1971, **13**(5), 316–329.
- 7 Weir, D. H. and Zellner, J. W. Lateral-directional motorcycle dynamics and rider control. *Society of Automotive Engineers Trans.*, 1979, 1364–1388.
- 8 Klein, R. E. Using bicycles to teach systems dynamics. *IEEE Control Systems Mag.*, April 1989, 4–9.
- 9 Wu, J. C. and Liu, T. S. Stabilization control for rider-motorcycle model in Hamiltonian form. *Veh. Systems Dynamics*, 1996, **26**, 431–448.
- 10 Sharp, R. S. and Alstead, C. J. The influence of structural flexibilities on the straight-running stability of motorcycles. *Veh. Systems Dynamics*, 1980, **9**(6), 327–357.
- 11 Sharp, R. S. and Giles, C. G. Static and dynamic stiffness and deflection mode measurements on a motorcycle, with particular reference to steering behaviour. In *Road Vehicle Handling*, 1983, pp. 185–192 (Mechanical Engineering Publications, London).
- 12 Liu, T. S. and Chen, J. S. Nonlinear analysis for motorcycle-rider systems. *Int. J. Veh. Des.*, 1992, **13**(3), 276–294.
- 13 Kortum, W. and Sharp, R. S. Multibody computer codes. *Veh. Systems Dynamics*, Suppl., 1993, **22**.
- 14 Lopez-Linares, S., Konno, A. and Uchiyama, M. Vibration controllability of flexible manipulators. *Trans. ASME, J. Dynamic Systems Measmt Control*, 1997, **119**, 326–330.
- 15 Ackermann, J. *Robust Control: Systems with Uncertain Parameters*, 1993 (Springer-Verlag, London).
- 16 Seffen, K. A. Bicycle-rider dynamics: equations of motion and controllability. Technical Report, UMIST/ME/AM/15.07.99/CUED, CUED/C-STRUCT/TR79, University of Manchester Institute of Science and Technology and Department of Engineering, University of Cambridge, 1999.
- 17 Grappe, F., Candau, R., Belli, A. and Rouillon, J. D. Aerodynamic drag in field cycling with special reference to the Obree's position. *Ergonomics*, 1997, **40**(12), 1299–1311.
- 18 Hucho, W. H. and Sovran, G. Aerodynamics of road vehicles. *A. Rev. Fluid Mechanics*, 1993, **25**, 485–537.
- 19 Soden, P. D. and Adeyefa, B. A. Forces applied to a bicycle during running. *J. Biomechanics*, 1979, **12**, 527–541.
- 20 Wang, E. L. and Hull, M. L. A model for determining rider induced energy losses in bicycle suspension systems. *Veh. Systems Dynamics*, 1996, **25**(3), 223–246.
- 21 Wang, E. L. and Hull, M. L. Minimization of pedaling induced energy losses in off-road bicycle rear suspension systems. *Veh. Systems Dynamics*, 1997, **28**(4), 291–306.
- 22 Sygne, J. L. and Griffith, B. A. *Principles of Mechanics*, 3rd edition, 1970 (McGraw-Hill, New York).
- 23 *MATLAB, Version 5.1*, 1998 (The MathWorks Inc., Natick, Massachusetts).

- 24 **Friedland, B.** *Control System Design: An Introduction to State-Space Methods*, 1986 (McGraw-Hill, New York).
- 25 **Newland, D. E.** *Mechanical Vibration Analysis and Computation*, 1989 (Longman, London).
- 26 **Friedland, B.** Controllability index based on conditioning number. *Trans. ASME, J. Dynamic Systems Measmt Control*, 1975, **97**(4), 444–445.
- 27 **Moore, B. C.** Principal component analysis in linear systems: Controllability, observability, and model reduction. *IEEE Trans. Autom. Control*, 1981, **AC-26**(1), 17–32.
- 28 **Furuta, K., Hiroyuki, K. and Kazuhiro, K.** Digital control of a double inverted pendulum on an inclined rail. *Int. J. Control*, 1980, **32**(5), 907–924.
- 29 **Suppaitnarm, A., Seffen, K. A., Parks, G. T., Connor, A. M. and Clarkson, P. J.** Multiobjective optimisation of bicycle frames using simulated annealing. In *Proceedings of the First ASMO–ISSMO Conference on Engineering Design Optimization* (Ed. V. V. Toporov), 1999, pp. 357–364.
- 30 **Richards, R. J.** *An Introduction to Dynamics and Control*, 1979 (Longman, London).
- 31 **Whitt, F. R. and Wilson, D. G.** *Bicycling Science*, 2nd edition, 1995 (MIT Press, Cambridge, Massachusetts).

## APPENDIX

### Lagrangian and equations of motion

For a rigid body of mass  $M$ , moving in space with centre-of-mass velocity  $\mathbf{v}$  and having angular velocity  $\boldsymbol{\Omega}$ , the kinetic energy has the following expression:

$$T = \frac{1}{2} M \mathbf{v}^2 + \frac{1}{2} (I_{xx} \Omega_{xx}^2 + I_{yy} \Omega_{yy}^2 + I_{zz} \Omega_{zz}^2) - (I_{xy} \Omega_{xx} \Omega_{yy} + I_{xz} \Omega_{xx} \Omega_{zz} + I_{yz} \Omega_{yy} \Omega_{zz}) \quad (11)$$

Axes  $Oxyz$  are attached to the centroid and have angular velocity components  $\Omega_{xx}$ ,  $\Omega_{yy}$  and  $\Omega_{zz}$  along the  $Ox$ ,  $Oy$  and  $Oz$  axes respectively, referred to a set of inertial axes. The terms in parentheses are due to rotational kinetic energy; the quantities  $I_{xx}$ ,  $I_{yy}$  and  $I_{zz}$  are the moments of inertia about the respective axes, and  $I_{xy}$ ,  $I_{xz}$  and  $I_{yz}$  are the products of inertia with respect to the chosen body-fixed axes.

For the rear frame, the kinetic energy with respect to lateral speed  $\dot{y}$ , yaw-rate  $\dot{\psi}$ , angle of steer  $\delta$  and lean angle from vertical  $\phi$  is given by

$$T_r = \frac{1}{2} M_r [(v - \psi h_r \sin \phi)^2 + (\dot{y} + \dot{\phi} h_r \cos \phi)^2 + \dot{\phi}^2 h_r^2 (\sin \phi)^2] + \frac{1}{2} I_{rxx} \dot{\phi}^2 + \frac{1}{2} I_{ryy} \dot{\psi}^2 (\sin \phi)^2 + \frac{1}{2} I_{rzz} \dot{\psi}^2 (\cos \phi)^2 - I_{rxz} \dot{\phi} \dot{\psi} \cos \phi \quad (12)$$

after Sharp [6] and then Seffen [16], and products of inertia transverse to the longitudinal plane are ignored. Likewise, for the lower torso and upper torso,

$$T_1 = \frac{1}{2} M_1 [(v - \psi h_1 \sin \phi)^2 + (\dot{y} + \dot{\phi} h_1 \cos \phi - \dot{\psi} p_1)^2 + \dot{\phi}^2 h_1^2 (\sin \phi)^2] + \frac{1}{2} I_{1xx} \dot{\phi}^2 + \frac{1}{2} I_{1yy} \dot{\psi}^2 (\sin \phi)^2 + \frac{1}{2} I_{1zz} \dot{\psi}^2 (\cos \phi)^2 - I_{1xz} \dot{\phi} \dot{\psi} \cos \phi \quad (13)$$

and

$$T_u = \frac{1}{2} M_u [(v - \psi h_u \sin \phi)^2 + (\dot{y} + \dot{\phi} h_u \cos \phi - \dot{\psi} p_u)^2 + (\dot{\phi} h_u \sin \phi)^2] + \frac{1}{2} I_{uwx} \dot{\phi}^2 + \frac{1}{2} I_{uyy} \dot{\psi}^2 (\sin \phi)^2 + \frac{1}{2} I_{uzz} \dot{\psi}^2 (\cos \phi)^2 - I_{uzx} \dot{\phi} \dot{\psi} \cos \phi \quad (14)$$

The steering set has the kinetic energy

$$T_f = \frac{1}{2} M_f [v - \psi (a \sin \phi \sin \epsilon + e \sin \phi \cos \delta \sin \epsilon + e \cos \phi \sin \delta + f \sin \phi \cos \epsilon) - \dot{\delta} e \cos \epsilon \sin \delta]^2 + \frac{1}{2} M_f [\dot{y} + \dot{\phi} (a \cos \phi \sin \epsilon + e \cos \phi \cos \delta \sin \epsilon - e \sin \phi \sin \delta + f \cos \phi \cos \epsilon) + \dot{\psi} (a \cos \epsilon + e \cos \delta \cos \epsilon - f \sin \epsilon) + \dot{\delta} (e \cos \phi \cos \delta - e \sin \phi \sin \delta \sin \epsilon)]^2 + \frac{1}{2} M_f [\dot{\phi} (a \sin \phi \sin \epsilon + e \sin \phi \cos \delta \sin \epsilon + e \cos \phi \sin \delta + f \sin \phi \cos \epsilon) + \dot{\delta} (e \sin \phi \cos \delta + e \cos \phi \sin \delta \sin \epsilon)]^2 + \frac{1}{2} I_{fxx} [\dot{\phi} \cos \epsilon \cos \delta + \psi (\sin \phi \sin \delta - \cos \phi \sin \epsilon \cos \delta)]^2 + \frac{1}{2} I_{fyy} [-\dot{\phi} \cos \epsilon \sin \delta + \psi (\sin \phi \cos \delta + \cos \phi \sin \epsilon \sin \delta)]^2 + \frac{1}{2} I_{fzz} [\dot{\phi} \sin \epsilon + \psi \cos \phi \cos \epsilon + \dot{\delta}]^2 - I_{fzx} [\dot{\phi} \cos \epsilon \cos \delta + \psi (\sin \phi \sin \delta - \cos \phi \sin \epsilon \cos \delta)] \times (\dot{\phi} \sin \epsilon + \psi \cos \phi \cos \epsilon + \dot{\delta}) \quad (15)$$

where the local body axes  $Oxyz$  now have  $Oz$  aligned parallel to  $SS$  [Fig. 1b(i)], the axis of steer. The kinetic energies due to a relative spin of the front and rear wheels are respectively given by

$$T_{fw} = i_{fwy} \{ [-\dot{\phi} \cos \epsilon \sin \delta + \psi (\sin \phi \cos \delta + \cos \phi \sin \epsilon \sin \delta)] \dot{\theta}_f + \frac{1}{2} \dot{\theta}_f^2 \} \quad (16)$$

and

$$T_{rw} = i_{rwy} (\dot{\theta}_r \dot{\psi} \sin \phi + \frac{1}{2} \dot{\theta}_r^2) \quad (17)$$

with  $\theta_f$  as the angular displacement of the front wheel

and, correspondingly,  $\theta_r$  for the rear wheel. The total gravitational potential energy  $V$  is directly stated as

$$\begin{aligned} V = & M_r g h_r \cos \phi + M_f g \\ & \times (a \cos \phi \sin \epsilon + e \cos \phi \cos \delta \sin \epsilon \\ & - e \sin \phi \sin \delta + f \cos \phi \cos \epsilon) \\ & + M_u g h_u \cos \phi + M_l g h_l \cos \phi \end{aligned} \quad (18)$$

where  $g$  is the acceleration due to gravity. The Lagrangian,  $\mathcal{L}$ , may now be completely specified by

$$\mathcal{L} = T_r + T_{rw} + T_f + T_{fw} + T_u + T_l - V \quad (19)$$

The equations of motion are derived by application of Lagrange's equations [22]. For generalized coordinates  $\delta$  and  $\phi$  the standard form of equations apply:

$$\frac{d}{dt} \left( \frac{\partial \mathcal{L}}{\partial \dot{q}_i} \right) - \frac{\partial \mathcal{L}}{\partial q_i} = Q_i \quad (20)$$

For quasi-coordinates  $\dot{y}$  and  $\dot{\psi}$ , more specific variants are required, namely, for the lateral equation of motion

$$\frac{d}{dt} \left( \frac{\partial \mathcal{L}}{\partial \dot{y}} \right) + \dot{\psi} \frac{\partial \mathcal{L}}{\partial v} = Q_1 \quad (21)$$

where  $Q_1$  is the generalized lateral force. For the yawing equation of motion use

$$\frac{d}{dt} \left( \frac{\partial \mathcal{L}}{\partial \dot{\psi}} \right) + \dot{y} \frac{\partial \mathcal{L}}{\partial v} - v \frac{\partial \mathcal{L}}{\partial \dot{y}} = Q_\psi \quad (22)$$

The coordinates  $\theta_f$  and  $\theta_r$ , and their derivatives with respect to time, are eliminated through the requirement of no longitudinal slip at each wheel. The generalized forces in each equation are approximated by

$$\begin{aligned} Q_1 & \approx Y_f + Y_r \\ Q_\psi & \approx LY_f - bY_r \\ Q_\delta & \approx -t_r[Y_f + Z_f(\phi + \delta \sin \epsilon)] + \tau_s - \gamma_s \delta \\ Q_\phi & \approx -t_r Z_f \delta \end{aligned} \quad (23)$$

$Z_f$  is the vertical reaction at the front wheel and  $\gamma_s$  is a steer damper that opposes the steer torque. The instantaneous side forces at the front and rear wheels are  $Y_f$  and  $Y_r$  and are developed from linear functions of angle of side slip and of camber such that

$$\begin{aligned} Y_r & = C_{rs} \left( \frac{b\dot{\psi} - \dot{y}}{v} \right) + C_{rc} \phi \\ Y_f & = C_{fs} \left( \delta \cos \epsilon - \frac{\dot{y} + \psi L - \delta t_r}{v} \right) + C_{fc} (\phi + \delta \sin \epsilon) \end{aligned} \quad (24)$$

$C_{fs}$  and  $C_{rs}$  are the front and rear tyre cornering stiffnesses and  $C_{fc}$  and  $C_{rc}$  are their camber stiffnesses;

Table 2 lists values that were found in the book by Whitt and Wilson [31].

Compounding terms in equations (2) to (4) are now explained. The overall mass of the system is

$$M = M_f + M_r + M_l + M_u \quad (25)$$

and the lever arm of the first moment of mass of the system normalized by  $M$  about a vertical axis through  $M_r$  is

$$p = \frac{1}{M} (M_f p_f - M_u p_u - M_l p_l) \quad (26)$$

Likewise, about a longitudinal horizontal axis in the ground plane through  $O'$ ,

$$h = \frac{1}{M} (M_f h_f + M_r h_r + M_l h_l + M_u h_u) \quad (27)$$

The mass  $M_j$  is derived from

$$M_j g e = M_f g e + M \frac{t_r (b + p) g}{w} \quad (28)$$

where  $e$  is the distance of  $M_f$  normal to, and in front of the steer axis [Fig. 1b(i)] and  $w$  is the wheelbase length. Lowell and McKell [5], for a simpler system idealization, identified a reduced form of the above expression as 'Jones's couple' after analysis by Jones [2] into self-righting mechanisms in bicycles. More specifically, equation (28) corresponds to a gravitational couple applied to the steering set per unit angle of rear frame lean. The moment of inertia of steering set about SS is

$$I_{fss} = I_{fzz} + M_f e^2 \quad (29)$$

and  $r$  is defined by the expression

$$\frac{I_{fss}}{r} = \frac{i_{fwy}}{R_f} + \frac{\lambda i_{rwy}}{R_r} \quad (30)$$

where  $\lambda$  is a dimensionless quantity that accounts for the transverse spin inertia of the engine flywheel-(pedal-crank-gear) assembly. In addition,

$$I_1 = M_f e p_f + I_{fzz} \cos \epsilon + I_{fzx} \sin \epsilon \quad (31)$$

and

$$I_2 = M_f e h_f + I_{fzz} \sin \epsilon - I_{fzx} \cos \epsilon \quad (32)$$

The total yaw and lean moments of inertia, and associated product of inertia, for a set of axes at  $O'$  are respectively given by

$$I_{O'zz} = M_f p_f^2 + M_u p_u^2 + M_1 p_1^2 + I_{rzz} + I_{fxx} (\sin \epsilon)^2 \\ + I_{fzz} (\cos \epsilon)^2 + I_{fzx} \sin(2\epsilon) + I_{uzz} - I_{lzz} \quad (33)$$

$$I_{O'xx} = M_r h_r^2 + M_f h_f^2 + M_u h_u^2 + M_1 h_1^2 + I_{fzz} (\sin \epsilon)^2 \\ + I_{fxx} (\cos \epsilon)^2 - I_{fzx} \sin(2\epsilon) + I_{rxx} + I_{uxx} + I_{lxx} \quad (34)$$

$$I_{O'xz} = -M_f p_f h_f + M_u p_u h_u + M_1 p_1 h_1 + (I_{fxx} - I_{fzz}) \\ \times \sin \epsilon \cos \epsilon + I_{fzx} \cos(2\epsilon) + I_{rxz} + I_{uxz} + I_{lxz} \quad (35)$$

Finally,

$$C_1 = C_{fs} + C_{rs}, \quad C_2 = \frac{bC_{rs} - LC_{fs}}{w}$$

$$C_3 = C_{fs} \cos \epsilon + C_{fc} \sin \epsilon, \quad C_4 = C_{fc} + C_{rc}$$

$$C_5 = \frac{b^2 C_{rs} + L^2 C_{fs}}{w^2}, \quad C_6 = \frac{LC_{fc} - bC_{rc}}{w} \quad (36)$$

$C_1$  to  $C_6$  are in newtons per radian.